PAPER • OPEN ACCESS

A procedure for the dynamic range characterization of X-ray imaging linear and TDI detectors

To cite this article: Alessandro Re *et al* 2024 *JINST* **19** C10005

View the article online for updates and enhancements.

A procedure for the dynamic range characterization of X-ray imaging linear and TDI detectors

Alessandro Re [a,b,*] **Niccolò Peruzzi,** [a,d] **Filippo Del Greco,** [a] **Marco Nervo,** [c,b]
Nadia Pastrone, [b] **Roberto Sacchi** [a,b] **and Alessandro Lo Giudice** [a,b]

[a]*Dipartimento di Fisica, Università di Torino,*
via Pietro Giuria 1, 10125 Torino, Italy

[b]*Istituto Nazionale di Fisica Nucleare, Sezione di Torino,*
via Pietro Giuria 1, 10125 Torino, Italy

[c]*Centro Conservazione Restauro "La Venaria Reale",*
Via XX Settembre 18, 10078 La Venaria Reale, Torino, Italy

[d]*Medical Radiation Physics, Department of Clinical Sciences Lund, Lund University,*
Barngatan 4, 22242 Lund, Sweden

E-mail: alessandro.re@to.infn.it

ABSTRACT: This paper presents a methodology to fully characterize the dynamic range of a linear X-ray detector, usually employed to perform radiography and tomography. The proposed procedure analyzes each pixel of the detector and presents the results both in terms of general performance of the detector and as a spatial distribution of different parameters for each pixel. This method has been applied to three X-ray detectors: one linear and two TDI (Time Delay Integration) detectors, used to implement X-ray imaging setups inside the neu_ART project. The results obtained from this characterization, carried out in experimental conditions typically employed during real X-ray imaging experiments, allow to completely determine the behavior and the limits of the detectors and to optimize the procedure used to acquire radiographic and tomographic data, especially in terms of determining the maximum exposure time that can be used to achieve the best signal quality with a faster acquisition.

---

*Corresponding author.

Contents

1 Introduction

Scientific and technological applications in the field of Cultural Heritage (CH) analysis are of utmost importance to preserve and increase the knowledge about our heritage. Especially because of the uniqueness of artworks and archaeological materials, it is desirable to use non-invasive techniques for their study and characterization. Most of these techniques are based on the interaction of particles with the materials under study, analyzing the products of the interactions or the modification of the impinging beam after the interaction. Our group has been working on these topics for many years, choosing probes and analytical techniques on the basis of specific problems to be solved (e.g. proton [1], neutron [2] or photon [3] probes) and even developing new instrumentation when this was not yet available [4].

This approach led to the neu-ART project [5], where we designed and developed unique setups to perform X-ray imaging on CH materials using "X-ray scanners", i.e. by moving a linear detector behind the artwork (that can be large up to some meters), without touching it and acquiring a radiograph in a fast way [6]. A rotating platform below the artwork allows the acquisition of many radiographs at different angles, and, by combining them, a tomography can be obtained. The developed setups have already been used to analyze many artworks of different materials and sizes [7–9]. To the best of our knowledge, this is the first time that this approach has been developed to acquire X-ray images of CH materials; in fact, experimental setups usually make use of area detectors, both active [10] or based on a scintillator/ mirror/ camera equipment [11]. When using these methods, either the objects are smaller than the active area of the detector [12], or a long stitching work to join different acquisitions is needed [13]. In this paper we focus on the detectors chosen for the neu_ART setups. We propose a procedure to fully characterize the dynamic range of a CCD-based detector and we apply it to characterize our instrumentation.

2 Experimental setup

The three detectors that have been selected for this project are linear and TDI (Time Delay Integration) X-ray detectors by Hamamatsu Photonics. They are usually employed in security scanners for luggage or to acquire radiographs of objects moving on a conveyor belt. In our application, the object to be analyzed is standing still, while the detector, oriented vertically, is moving horizontally behind it. Behind each detector, we installed a set of heatsinks each coupled with a fan (from 3 to 6, depending

on the size of the detector case) to cover most of its back surface, so that the heat generated by the electronics is quickly dissipated in the air, and the temperature of the detector is kept constant during all the acquisitions. The characteristics of the three detectors are presented in table S1 of the supplementary data. The linear detector is composed of a single column of pixels, while TDI detectors are area detectors where multiple columns of pixels are arranged in a row (128 pixels wide). In TDI operating mode, the stack of linear arrays is aligned with and synchronized to the motion of the detector in such a way that, as the detector moves along its track, the integrated charge steps along with it. Compared to a single linear detector, this approach provides higher signal intensity with the same exposure time, thus allowing for smaller pixel sizes and shorter acquisition times.

The linear detector C9750-20TCN has been selected because of its considerably long sensor strip and relatively small pixel size: this is a good compromise to scan large areas in a short time and to obtain radiographs with sizes that can be managed with ordinary computers. Moreover, the wide range of detectable energies allows for the analysis of objects of very different materials and scale. The TDI C10650-321 has been selected to analyze smaller objects or details of larger objects with an increased resolution compared to the linear instrument. The lower value of maximum energy may sound like a limitation, but since better resolution is typically needed for smaller objects, which require lower energies to be analyzed, this is not a problem in most of the situations. A drawback of this detector is that it is composed of three different sensors, mounted on top of each other with a small discontinuity. This causes two dead areas, corresponding to the size of a few pixels, that creates the effect of missing lines in the radiograph; although this does not change the general view, it can be noticed at high magnification. The TDI C10650-461 is an upgrade of the previous detector, which circumvents the problem. It is longer and is composed of 4 sensors. Here there are no dead areas, because the sensors are staggered and the overlapping zone between any two is acquired by both and combined by a software in the post-production phase. Moreover, the analog to digital (A/D) conversion depth of this detector is 16 bits (compared to 12 bits of the previous detectors), potentially increasing the number of detectable gray levels.

The data presented in the following have been obtained using Eresco X-ray sources from General Electrics, under conditions and geometry typically employed during real X-ray imaging experiments with these setups: the voltage ranged from 60 to 100 kV, the current was set almost at the maximum available for the selected voltage and a 2 mm thick aluminum filter was placed in front of the source. The emerging X-ray spectrum was continuum, with a maximum energy value related to the corresponding voltage (60 to 100 keV), the low energies contribution absorbed by the Al filter and the characteristic emissions of the tungsten anode (in the range 60–70 keV) superimposed. Each detector was placed at around 3.5 meters from the source and kept fixed with its center in front of the focal spot, so that, even if the source generated a cone-beam, the distance caused the X-ray beam to hit with almost uniform intensity the whole area of the detector.

3 Procedure for the characterization of a detector

In this study we define a procedure to fully characterize the dynamic range of a CCD-based detector. The work is based on the procedure proposed in [14] to study a small area of a flat panel X-ray detector. We already successfully tested this procedure on neutron detectors integrating scintillator, mirror and camera [15], but for this work we extended the method to be applied to a linear detector and to study all the pixels individually.

The real dynamic range, or signal depth resolution, of a detector can be defined as the number of effectively discernible gray levels after signal quantization and is in general much lower than the number of values provided by the analog-to-digital converter (ADC). It depends on several features of both the detector and the converter, such as noise and linearity [16–18]. The number of bits of the ADC is the quantity reported by the vendors, but it is not representative of how wide the dynamic range of the detector is, i.e. how many different input signals can be separated with it [14]. In X-ray imaging (both digital radiography and tomography) it is important to have a wide dynamic range because this means having a good contrast. If a CCD is used to measure the X-ray absorption, as it happens in digital radiography or in computed tomography, each one of the CCD's pixels can record a signal level from dark current level, or baseline level, to saturation level. Usually one speaks about background noise of a CCD referring to the noise at the dark current level, which is the average fluctuation (standard deviation) in the dark current of the readout electronics of the sensor. If we are talking about noise at other levels we should refer to it as bright noise, as it is dominated by fluctuations in the signal collection process rather than by the readout electronics [14]. Fluctuations on the collected signal for rays of a given energy produce an uncertainty band around the average value, and it is possible to quantify the amplitude of this band by computing the standard deviation of the signal. We may call this characteristic noise-band, or simply noise. If two signals intensities are very close to each other and we want to separate them, they must have at least a difference larger than the noise-band [14]. It is clear that, for this reason, the noise limits the amount of gray levels that can be distinguished one from the other, and as such needs to be taken into account when one calculates the dynamic range.

For a constant noise, the dynamic range (DR) is defined as $DR = 20 \log(S/N)$, where DR is the dynamic range in decibel, N is the average amplitude of noise and S is the maximum signal, or the amplitude of the useful signal range [14]; the last two are typically expressed in ADC bit units. Here S/N can be interpreted as the number of effective distinguishable signal levels. Since in our application N depends on the signal S ($N = N(S)$), an integration is needed to account for the varying noise amplitude when computing the dynamic range. The definition of the number of effectively available levels should be extended as: $L = \int_a^b dS/N(S)$, where a and b are the lower and the upper limits of the useful signal range respectively and $N(S)$ is the noise amplitude as a function of the signal. This function is not known a priori and has to be determined by interpolating a set of values measured experimentally [14]. Our experimental procedure consisted in collecting a set of 20 images in the following range of exposure times (corresponding to different acquisition rates in lines/minute) for each detector: from 0.24 to 24 ms for the linear detector; from 56.7 to 1843 ms for the C10650-321 TDI detector; from 61.44 to 1843.2 ms for the C10650-461 TDI detector. The values were selected in order to cover the full range from baseline to saturation, using irradiating conditions and distance typically employed during real X-ray imaging experiments with these setups. On TDI devices longer exposure times account for a lower luminosity mainly due to smaller pixel areas. To avoid systematic effects, due to long term drifts of the signal, the sequences of the 20 acquisition times were randomly ordered, not starting from the minimum and then gradually increasing or, conversely, starting from the maximum and then gradually decreasing. For each exposure time, two images were acquired: one with the source on (in the following called W or white) and one with the source off (in the following called D or dark). To achieve good statistics, for each image 1000 lines were sampled (corresponding to 1000 acquisitions for each pixel). It is worth to notice that, for the TDI detectors, the 128 sensor pixels in the same row all contribute to the gray value of the same pixel in the final image, so from

now on we will use the word "pixel" also for the TDI, referring to the sum of the signal integrated, moved and transferred by the 128 elements of the same row. Both the signal average and the standard deviation were calculated for each pixel from the 1000 values acquired. The average was assumed as the signal value S and the standard deviation as the noise width N.

The images used for the characterization were acquired using Hipic, the software delivered by the detector manufacturer, and were processed using Matlab routines expressly written to automate the procedure for the analysis of each pixel. The characterization of the detectors has been carried through the following steps: Signal stabilization; Dark current sampling; Detector Response determination; Signal to Noise ratio calculation; Dynamic range characterization. Only the last step is reported in the following section, but the details of all the other steps for our procedure are reported in the supplementary data. The dynamic range characterization is based on all the previous evaluations. The procedure for this latter step is the same reported in [14], which we briefly summarize in the following. The $1/N$ data as a function of the signal S, measured as W-D, are fitted with a power function, whose exponent is expected to be close to -0.5 (i.e. purely Poisson distribution). The dynamic range is obtained by the integration of this curve between the two limits corresponding to the baseline and the saturation. In figure S6 in the supplementary data, an example of this curve is shown for one pixel of the linear detector. Also in this case the fitting curve is a power function: $1/N = c \cdot S^d$ where the value for the d parameter would be -0.5, if the Poisson contribution was present alone. The integration of this curve between 0 and ($Imax - D$) (where $Imax$ is 4095 for the linear and TDI-C10650-321 detectors and 65535 for the TDI-C10650-461 detector representing the nominal amount of ADC levels), gives the number of distinguishable levels L for each pixel. To evaluate the uncertainty on L values, we also integrated the maximum and minimum curves fitting each dataset (taking into account the uncertainties associated with the fit parameters): the uncertainty on L was then fixed as the maximum among the absolute deviations between the best fit and the maximum and minimum curves respectively. Even if this is an overestimation of the uncertainty, it is easy to calculate and integrate in the routine for the analysis of each pixel. The dynamic range DR can then be easily derived as $DR = 20 \log(L)$.

4   Results

The parameter L, estimated for each pixel, allows us to evaluate the effective quality of the detector and to compare its performance to the one of other detectors (figure 1). In the linear detector, the median of the resulting values is 180 effective gray levels, but varying results for different pixels suggest the presence of multiple adjacent pixel groups, with even more homogeneous values within each of them. This likely represents the internal organization of the detector's electronics, possibly built with modular components.

The TDI-C10650-321 shows a wide distribution of the L values (from about 160 to 490 effective gray levels), similarly distributed as large bands, with better performance in the central of the three evidently visible sections composing the detector.

The TDI-C10650-461 shows a bimodal distribution of the L values, one with the median at 670 effective gray levels and the other at 830. This double behavior is easily explained by looking at the spatial distribution of the values: the two central arrays in which the detector is subdivided perform consistently better than the lateral ones, which may be either a coincidence or a deliberate manufacturing choice, given that a comparable outcome was obtained for both TDI detectors. One potential explanation is that the central portion of an imaging detector is generally the most exploited
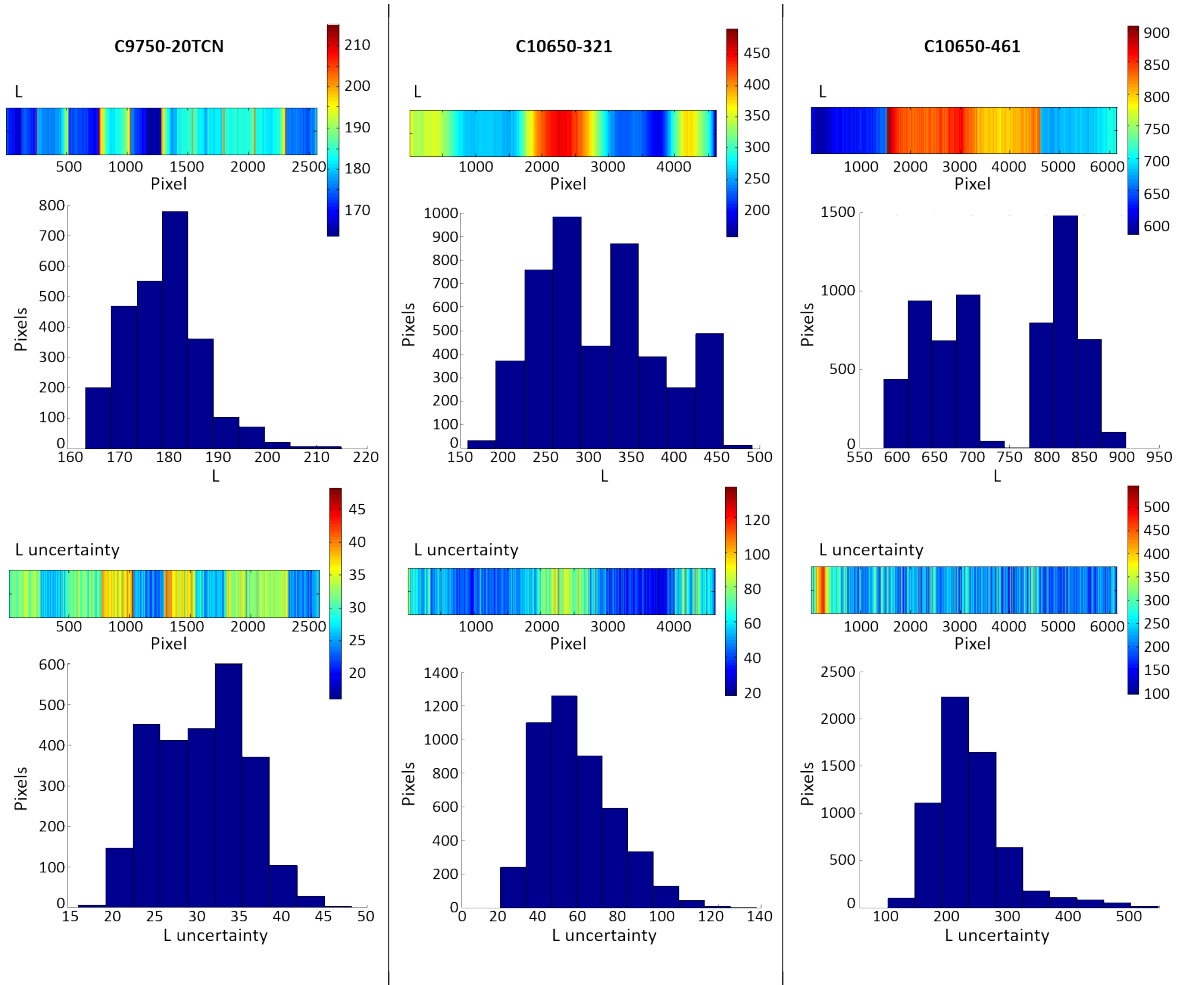
Figure 1. Evaluation of the effective gray levels (L) for each pixel of the 3 detectors: in the upper part the spatial distributions of the L value and the histograms of L values are represented. In the lower part the same is represented for L uncertainty.

(in a radiograph, the object under analysis is typically positioned in the center), and it is therefore preferable to have the most performing part of the detector in that location.

The dynamic range results obtained for all the 3 detectors are summarized in table 1, where both the effective gray levels and its uncertainty are evaluated as the medians of the histograms shown in figure 1.

Table 1. Parameters evaluated from the characterization compared to the number of ADC channels.

Parameters	Hamamatsu C9750-20TCN	Hamamatsu C10650-321	Hamamatsu C10650-461
ADC channels	4096 (12 bit)	4096 (12 bit)	65536 (16 bit)
Effective gray levels range	164 ÷ 215	159 ÷ 492	582 ÷ 906
Effective gray levels median	180 ±30	300 ±50	670 ±220; 830 ±230
Real Dynamic range (dB)	45	50	56; 58

5 Conclusions

A method to fully characterize the dynamic range of a linear detector has been developed and presented. The method analyzes each pixel individually, giving a clear idea of a detector performances in terms of homogeneity and real dynamic range. From the results of the characterization some important information about the use of the detector during X-ray imaging acquisitions can be obtained.

The proposed method has been applied to three detectors, one linear and two TDI, acquired for the implementation of X-ray radiography and tomography setups, mainly devoted to the analysis of CH materials. From this characterization, the effective gray level amount and the real dynamic range have been obtained for each device. The homogeneity in the response has been evaluated and some indication about the use of these detectors has been highlighted, especially in terms of determining the maximum exposure time that can be used to achieve the best signal quality with a faster acquisition.

Acknowledgments

References

[1] L. Guidorzi et al., *Micro-PIXE and micro-IBIL characterization of lapis lazuli samples from Myanmar mines and implications for provenance study*, *Eur. Phys. J. Plus.* **138** (2023) 175.

[2] N. Gelli et al., *The new INFN-CHNet neutron imaging facility*, *Nucl. Instrum. Meth. A* **1051** (2023) 168189.

[3] J. Corsi et al., *Potentialities of X-ray fluorescence analysis in numismatics: the case study of pre-Roman coins from Cisalpine Gaul*, *Archaeol. Anthropol. Sci.* **10** (2018) 431.

[4] A. Re et al., *Towards a portable X-ray luminescence instrument for applications in the Cultural Heritage field*, *Eur. Phys. J. Plus.* **133** (2018) 362.

[5] M. Nervo, *Cronache 4: Il Progetto neu_ART. Studi e applicazioni. Neutron and X-ray tomography and imaging for cultural heritage*, Editris, Brezzo di Bedero (2013).

[6] A. Lo Giudice et al., *A new digital radiography system for paintings on canvas and on wooden panels of large dimensions*, in the proceedings of the *2017 IEEE International Instrumentation and Measurement Technology Conference (I2MTC)*, Turin, Italy (2017), p. 1–6 [DOI:10.1109/I2MTC.2017.7969985].

[7] L. Vigorelli et al., *X-ray Micro-Tomography as a Method to Distinguish and Characterize Natural and Cultivated Pearls*, *Condens. Mat.* **6** (2021) 51.

[8] L. Vigorelli et al., *The study of ancient archaeological finds through X-ray tomography: the case of the "Tintinnabulum" from the Museum of Anthropology and Ethnography of Torino*, *J. Phys. Conf. Ser.* **2204** (2022) 012034.

[9] A. Re et al., *The importance of tomography studying wooden artefacts: a comparison with radiography in the case of a coffin lid from Ancient Egypt*, *Int. J. Conserv. Sci.* **7(SI2)** (2016) 935.

[10] C. Tuniz et al., *The ICTP-Elettra X-ray laboratory for cultural heritage and archaeology*, *Nucl. Instrum. Meth. A* **711** (2013) 106.

[11] M.P. Morigi et al., *Application of X-ray Computed Tomography to Cultural Heritage diagnostics*, *Appl. Phys. A* **100** (2010) 653.

[12] F. Bernardini et al., *Beeswax as Dental Filling on a Neolithic Tooth*, *PLoS ONE* **7** (2012) e44904.

[13] M. Bettuzzi et al., *Computed tomography of a medium size Roman bronze statue of Cupid*, *Appl. Phys. A: Materials Science & Processing* **118** (2015) 1161.

[14] M. Bettuzzi, R. Brancaccio, M.P. Morigi and F. Casali, *Effective dynamic range measurement for a CCD in full-field industrial x-ray imaging applications*, *Proc. SPIE* **6616** (2007) 66161L.

[15] E.A. Durisi et al., *Characterization of a neutron imaging setup at the INES facility*, *Nucl. Instrum. Meth. A* **726** (2013) 31.

[16] K. Irie, A.E. McKinnon, K. Unsworth and I.M. Woodhead, *A model for measurement of noise in CCD digital-video cameras*, *Meas. Sci. Technol.* **19** (2008) 045207.

[17] K. Irie et al., *A Technique for Evaluation of CCD Video-Camera Noise*, *IEEE Trans. Circuits Syst. Video Technol.* **18** (2008) 280.

[18] S.M. Gruner et al., *Charge-coupled device area x-ray detectors*, *Rev. Sci. Instrum.* **73** (2002) 2815.